Parallel Numerical Reservoir Simulations of Nonisothermal Compositional Flow and Chemistry

M. Delshad, SPE, **S.G. Thomas,** and **M.F. Wheeler,** SPE, The University of Texas at Austin

Summary

This paper describes an efficient numerical scheme for nonisothermal compositional flow coupled to chemistry. An iterative implicit-pressure/explicit-composition (IMPEC) method is applied to solve the flow problem using a volume-balance-convergence criterion. A backward-Euler mixed finite-element method (FEM) with lowest-order RT_0 elements is applied to solve the pressure equation, and a component local mass-preserving explicit scheme is used to update concentrations. Chemical reactions are solved using explicit Runge-Kutta (RK) ordinary-differential-equation (ODE) integration schemes. A higher-order Godunov method and a backward-Euler mixed FEM are applied for thermal advection and conduction, respectively, in a time-split scheme.

One of the major applications of the method is in the modeling of field-scale carbon dioxide (CO_2) sequestration as an enhanced-oil-recovery (EOR) process or for containment in deep saline aquifers where chemical reactions and temperature variations may have an effect on the flow and transport of CO_2. Leakage patterns when CO_2 is injected near leaky abandoned wells, the displacement of methane from depleted gas reservoirs, and accurate modeling of geochemical reactions involving injected CO_2 are other applications of interest.

Results of a benchmark problem in multiphase flow with several hydrocarbon components in formations with highly heterogeneous permeability on very fine grids, as well as a large-scale parallel implementation of modeling CO_2 sequestration, are presented to justify the practical use of the model. A parallel efficiency of approximately 80% was observed on up to 512 cores in the benchmark study. Results from a problem simulating injection of CO_2 in deep aquifers including nonisothermal and chemical effects are also presented. The results indicate a good agreement of the solutions with published data, where available.

Numerical modeling and simulation of CO_2 sequestration plays a major role in future site selections and in designing storage facilities for effective CO_2 containment. The main contribution of this paper lies in providing a parallel and efficient method of simulating challenging compositional flow problems, such as in the study of CO_2 sequestration, as well as flow coupled to thermal and geochemical effects.

Introduction

Field-scale modeling and simulation of CO_2 sequestration is emerging as an important research topic. Global warming of approximately 0.4 to 0.6°C observed over the course of the last century is attributable to the emission of greenhouse gases (mainly CO_2) from the fossil-fuel-consumption and energy-sector emissions (Bachu 2000). The sequestration of CO_2 into the subsurface is recognized as the most practically feasible means of addressing the global-warming threat posed to our planet. Furthermore, CO_2 flooding is recognized as a very efficient means of EOR in the petroleum industry. Hence, it is important to model accurately such features as the flow of CO_2 in the subsurface, duration and amounts sequestered, leakage rates when injected in the proximity of abandoned/leaky wells or in natural geological formations with faults, the shapes of CO_2 plumes as CO_2 moves and displaces methane and other natural gases in depleted gas reservoirs, and concentration of any products formed from chemical reactions, among other features.

Accurate modeling of flow scenarios where the nonaqueous phase is composed of several hydrocarbon components is not possible with a black-oil model. A compositional model is very valuable in modeling such real-world flow applications. For modeling thermal effects, nonisothermal fully implicit compositional models (Brantferger et al. 1991) can prove to be too expensive and almost infeasible when several hydrocarbon components are present on extremely fine grids. Similarly, fully implicit numerical solution of compositional flow coupled with thermal and geochemical effects is intractable. This paper describes an efficient numerical scheme for multiphase nonisothermal flow. In this work, an iteratively coupled IMPEC scheme is applied to solve the flow problem, which is then sequentially coupled to a time-split method for solving the thermal energy balance and an explicit ODE numerical integration method for chemical reactions.

The method for flow is related to some recent work (Chen et al. 2000, 2005, 2007) as well as older work (Coats 1980; Watts 1986; Acs et al. 1985). The scheme described here solves for concentrations and may be related to Picard's method of successive approximation for ODEs. The pressure system at every iteration is solved using a backward-Euler mixed FEM with suitable quadrature, reducing it to cell-centered finite differences. The concentrations are updated explicitly with a correction to preserve local component mass balance. The pressure/concentration system is then iteratively coupled until either the saturation constraint is satisfied within a tolerance or a maximum number of iterations is reached, whichever occurs first. The time-split scheme for thermal energy transfer is based upon a related idea for reactive transport applications (Dawson and Wheeler 1987). The idea is to account separately by accumulation for the contributions from thermal advection and conduction. A higher-order Godunov scheme is used for the advection step, and a fully implicit mixed method is used for the conduction step. Finally, higher-order RK methods are employed for chemistry.

The remainder of this paper is organized as follows. The following sections, in order, describe the basic equations governing the flow problem including the assumptions and some theory on the equation of state (EOS), with a brief discussion of the two-phase flash algorithm, the thermal-energy-balance problem, the equations governing chemistry, and a sequential coupling to flow and chemistry. Finally, some numerical results are presented for benchmark and practical real-world problems obtained using the coupled flow/thermal/chemistry source code developed within the Integrated Parallel and Accurate Reservoir Simulator v3 (IPARSv3) simulator framework (Wheeler 2001).

Compositional Flow Model

Let i and α represent component and phase indices, respectively. In the IPARSv3 simulator, $i = 1$ refers to the water component. Component mass balances for n_c components $i = 1, \ldots, n_c$ are then given by the system of partial-differential equations:

This paper (SPE 118847) was accepted for presentation at the SPE Reservoir Simulation Symposium, The Woodlands, Texas, USA, 2–4 February 2009, and revised for publication. Original manuscript received for review 3 November 2008. Revised manuscript received for review 4 June 2010. Paper peer approved 8 July 2010.

$$\frac{\partial(\phi N_i)}{\partial t}+\nabla\cdot\left(\sum_{\alpha}\mathbf{J}_i^{\alpha}\right)=q_i. \quad \ldots\ldots\ldots\ldots\ldots\ldots\ldots\ldots\ldots\ldots (1)$$

In Eq. 1, ϕ denotes the medium porosity and N_i and q_i represent the molar concentration and production (injection) rates at sources (sinks) of Component i, respectively. $\mathbf{J}_i^{\alpha}$ is the net velocity of Component i in Phase α given by

$$\mathbf{J}_i^{\alpha}=\rho_{\alpha}\xi_i^{\alpha}\mathbf{u}_{\alpha}-\phi\rho_{\alpha}S_{\alpha}\mathbf{D}_i^{\alpha}\nabla\xi_i^{\alpha}. \quad \ldots\ldots\ldots\ldots\ldots\ldots\ldots\ldots\ldots\ldots (2)$$

The definition of the diffusion/dispersion tensor $\mathbf{D}_i^{\alpha}$ can be found in Chen et al. (2006). Only molecular diffusion is considered in this work. This renders $\mathbf{D}_i^{\alpha}$ a diagonal tensor. In Eq. 2, ρ_{α}, S_{α}, and $\mathbf{u}_{\alpha}$ are the density, saturation, and velocity, respectively, of Phase α and ξ_i^{α} is the mole fraction of Component i in Phase α. The velocity $\mathbf{u}_{\alpha}$ is given by the well-known Darcy's constitutive law:

$$\mathbf{u}_{\alpha}=-\frac{\kappa_{r\alpha}}{\mu_{\alpha}}\mathbf{K}\left(\nabla p_{\alpha}-\gamma_{\alpha}\nabla D\right), \quad \ldots\ldots\ldots\ldots\ldots\ldots\ldots\ldots\ldots\ldots (3)$$

where $D(\mathbf{x})$ denotes the depth and is a function of the space variable. The phase pressures p_{α} may be eliminated in terms of the reference phase pressure p by the capillary pressure relation, which is assumed to be a known function of phase saturations, given by

$$p_{\alpha}=p+p_{c\alpha}\left(\{S_{\alpha}\}\right), \quad \ldots\ldots\ldots\ldots\ldots\ldots\ldots\ldots\ldots\ldots\ldots (4)$$

where α runs through all phase indices except that of the reference phase. In Eq. 3, $\mathbf{K}$ denotes the absolute permeability of the medium and μ_{α}, γ_{α}, and $\kappa_{r\alpha}$ denote the viscosity, specific gravity, and relative permeability of Phase α, respectively. It is assumed that $\kappa_{r\alpha}$ is a function of $\{S_{\alpha}\}$. The reference phase pressure is used in the flash, well, and geomechanical calculations. After linearization, the porosity may be expressed as

$$\phi=\phi_0\left[1+c_r\left(p-p_0\right)\right], \quad \ldots\ldots\ldots\ldots\ldots\ldots\ldots\ldots\ldots\ldots\ldots (5)$$

where c_r is the (constant) rock compressibility factor and ϕ_0 is the porosity at the prescribed standard pressure p_0.

In what follows, pure-component properties are expressed in terms of state variables p and T and their mole fractions ξ_i^{α} determined using thermodynamic equations for phase equilibrium (also termed the fugacity or flash equations), which, in turn, yield phase properties from appropriate mixing rules. Phase saturations are expressed in terms of the state variables $\left[p,\mathbf{N},\left\{\xi_i^{\alpha}\right\},T\right]^T$ (detailed in the EOS and Flash Implementation subsection). Then, the system needs to be decoupled and solved for the reference phase pressure p, component molar concentrations N_i, phase compositions $\left\{\xi_i^{\alpha}\right\}$, and the reservoir temperature T. To this end, an Arrhenius exponential temperature correlation of the form $\mu_w=\mu_{w,\mathrm{ref}}\exp b_w\left(\frac{1}{T}-\frac{1}{T_{\mathrm{ref}}}\right)$ is assumed to describe the water-phase viscosities μ_w, where $\mu_{w,\mathrm{ref}}$ is the reference viscosity of water prescribed at T_{ref} and b_w is a constant.

Similarly, the nonaqueous-phase viscosities μ_{α} appearing in Eq. 3 are calculated using a Lohrenz-Bray-Clark correlation. In this method, at low pressures, component viscosities are estimated using a Stiel and Thodos correlation in the form $\mu_i^{\mathrm{low}}=\frac{\beta_i}{\lambda_i}$, where β_i is a function of $T_{i,r}$ and λ_i is a function of $T_{i,cr}$ and $p_{i,cr}$. Similarly, at high pressures, a different correlation is used to obtain μ_i^{high}. Using the component values and an appropriate mixing rule, the phase viscosities are calculated. The terms $T_{i,cr}$, $p_{i,cr}$, and $T_{i,r}$ are explained in more detail in the EOS and Flash Implementation subsection. The nonaqueous-phase molar specific volumes (i.e., $v_{\alpha}\equiv 1/\rho_{\alpha}$) are given by the gas law:

$$\nu_{\alpha}=\frac{RTZ_{\alpha}}{p_{\alpha}}, \quad \ldots\ldots\ldots\ldots\ldots\ldots\ldots\ldots\ldots\ldots\ldots\ldots (6)$$

where R is the universal gas constant and Z_{α} is the Z factor (also called compressibility factor) of Phase α, obtained by solving the EOS. The aqueous-phase molar specific volume is given by

$$\nu_w=\frac{\nu_w^0 B_w^0}{1+c_w\left(p_w-p^0\right)}, \quad \ldots\ldots\ldots\ldots\ldots\ldots\ldots\ldots\ldots\ldots\ldots (7)$$

where c_w is the water-phase compressibility. p_w^0 is the standard water-phase pressure (usually 1 atm) at which the values ν_w^0 and B_w^0 of the molar specific volume and the formation volume factor, respectively, are prescribed. The phase saturations are then expressed in terms of the state variables, $\left[p,\mathbf{N},\left\{\xi_i^{\alpha}\right\},T\right]^T$, by the equations

$$S_w=\nu_w N_w,$$

$$S_l=(1-\nu)\nu_l\sum_{i=2}^{n_c}N_i,$$

and

$$S_g=\nu\nu_g\sum_{i=2}^{n_c}N_i, \quad \ldots\ldots\ldots\ldots\ldots\ldots\ldots\ldots\ldots\ldots\ldots\ldots (8)$$

where ν is the vapor fraction and the subscripts w, l, and g stand for the aqueous, oleic, and gaseous phases, respectively. The saturations calculated in Eq. 8 will not, in general, sum to unity; therefore, the iterative IMPEC method needs an additional constraint,

$$\sum_{\alpha}S_{\alpha}=1. \quad \ldots\ldots\ldots\ldots\ldots\ldots\ldots\ldots\ldots\ldots\ldots\ldots\ldots\ldots (9)$$

Eq. 9 is the familiar volume-balance criterion that forms the convergence condition for the iterative IMPEC method.

EOS and Flash Implementation. The IPARSv3 simulator uses a Peng-Robinson EOS (Peng and Robinson 1976) to determine the nonaqueous molar specific volumes of Eq. 6 in terms of the Z factors, which are functions of p and T. It can be shown (Chang 1990) that this reduces to solving a cubic equation for $\overline{Z}_{\alpha}$, which includes a volumetric shift parameter C_{α} so that $Z_{\alpha}=\overline{Z}_{\alpha}-C_{\alpha}$. The cubic EOS for Phase α then takes the form

$$\overline{Z}_{\alpha}^3+h_1\left(B_{\alpha}\right)\overline{Z}_{\alpha}^2+h_2\left(A_{\alpha},B_{\alpha}\right)\overline{Z}_{\alpha}+h_3\left(A_{\alpha},B_{\alpha}\right)=0. \quad \ldots\ldots\ldots (10)$$

The parameters A_{α} and B_{α} appearing in the coefficients h_j of the cubic Eq. 10 and the volumetric shift C_{α} in the definition of $\overline{Z}_{\alpha}$ are functions of the component reduced pressures and temperatures $\{p_{i,r}\}$ and $\{T_{i,r}\}$, where $p_{i,r}=p_i/p_{i,cr}$ and $T_{i,r}=T/T_{i,cr}$. They are also functions of the composition of that phase (by means of an appropriate mixing rule involving component mole fractions $\left\{\xi_i^{\alpha}\right\}$). It is noted that p_i is the partial pressure of Component i in Phase α given by Dalton's law of partial pressures and $p_{i,cr}$, $T_{i,cr}$ represent the component critical pressures and temperatures, which are thermodynamic properties unique to every chemical component. For a detailed discussion on these and related thermodynamic concepts, see Chang (1990). Eq. 10 is solved using the Newton-Raphson method for nonlinear equations until the change in $\overline{Z}_{\alpha}$ is less than a prescribed tolerance. When multiple real roots exit, the root resulting in lowest Gibbs free energy is taken.

Vapor fractions are determined using the Rachford-Rice equation. It is given by

$$\sum_i\frac{\left(K_i-1\right)z_i}{1+\left(K_i-1\right)\nu}=0. \quad \ldots\ldots\ldots\ldots\ldots\ldots\ldots\ldots\ldots\ldots (11)$$

In Eq. 11, z_i is the overall nonaqeous mole fraction of Component i and K_i is defined in Eq. 12. The fluid is a single-phase liquid when $\nu=0$ and is a single-phase vapor when $\nu=1$. Once ν is determined using Eq. 11, the component mole fractions in the liquid and vapor phases can be calculated from

$$\xi_i^l=\frac{z_i}{1+\left(K_i-1\right)\nu}, \quad \xi_i^g=K_i\xi_i^l. \quad \ldots\ldots\ldots\ldots\ldots\ldots\ldots (12)$$

For a given state, the equibrium phase composition $\left\{\xi_i^\alpha\right\}$ uses a flash algorithm. From thermodynamic principles, phase equilibrium at constant pressure and temperature requires that component fugacities in each of the nonaqueous phases be equal; i.e., for $i = 2, \ldots, n_c$,

$$f_i^g = f_i^l. \quad (13)$$

Instead of solving Eq. 13 for component fugacities, the simulator solves for $\ln(K_i)$, working with fugacity coefficients, $\Phi_i^\alpha \equiv \dfrac{f_i^\alpha}{\xi_i^\alpha p}$, instead of fugacities. This modifies Eq. 13 to

$$R_i \equiv \ln\left(\Phi_i^l\right) - \ln\left(\Phi_i^g\right) - \ln\left(K_i\right) = 0. \quad (14)$$

The $\ln\left(\Phi_i^\alpha\right)$ term in Eq. 14 is a function of Z_α, $\{\xi_i\}^\alpha$, and p_α for the case of the Peng-Robinson EOS. The flash algorithm then applies the Newton-Raphson method to find the root of Eq. 14. The basic steps of the flash algorithm are given next. For further details, see Chang (1990) and Firoozabadi (1999).

1. $p_\alpha(p)$, T, and z_i are known and remain constant during the flash calculation. A starting value of K_i is assumed given. Then, the Rachford-Rice Eq. 11 is solved for v.

2. Next, component mole fractions $\{\xi_i\}^\alpha$ in nonaqueous phases are determined using Eq. 12. Note that $\xi_w^l = \xi_w^g \equiv 0$ and $\xi_w^w \equiv 1$ are not of interest here.

3. The cubic Peng-Robinson EOS (Eq. 10) is then solved to obtain the phase Z factors Z_α. Then, using the p_α given and the Z_α and $\{\xi_i\}^\alpha$ just obtained, the logarithm of the fugacity coefficients $\ln\left(\Phi_i^\alpha\right)$ is calculated from their functional form $\ln\left(\Phi_i^\alpha\right) \equiv f\left(Z_\alpha, \left\{\xi_i\right\}^\alpha, p_\alpha\right)$.

4. Eq. 14 is checked for convergence [or if the trivial solution is encountered (i.e., when for all i, $K_i \equiv 1$ within a tolerance)] for the timestep in question. If not converged, the said equation is expanded in terms of $\delta[\ln(K_i)]$ to obtain an update for $\ln(K_i)$ and the algorithm continues (for the same timestep) from Step 1.

Iterative IMPEC Method. As indicated by Eq. 8, phase saturations are functions of the state variables $\left[p, \mathbf{N}, T, \left\{\xi_i^\alpha\right\}\right]^T$. The volume-balance condition at the $(k+1)$th iteration of the nth timestep is written as

$$S_\Sigma^{k+1} \equiv \sum_\alpha S_\alpha^{k+1} = 1. \quad (15)$$

Expanding S_Σ^{k+1} in a Taylor series about S_Σ^k up to the first-order terms yields the approximation

$$\frac{\partial S_\Sigma}{\partial p}\delta p + \sum_{i=1}^{n_c}\frac{\partial S_\Sigma}{\partial N_i}\delta N_i + \sum_{i=2}^{n_c}\frac{\partial S_\Sigma}{\partial\left(\ln K_i\right)}\delta\left(\ln K_i\right) = 1 - S_\Sigma^k. \quad (16)$$

It can be shown that the fugacity equations (Eq. 13) can be expanded in terms of δp, δN_i, and $\delta(\ln K_i)$, and this expansion can be rearranged to express $\delta(\ln K_i)$ in terms of δp and δN_i. This expression is then be substituted into Eq. 16, resulting in an equation in terms of δp and δN_i. The mass-balance equation (Eq. 1) is then expanded to express δN_i in terms of δp, which results in a single system for cell pressure changes of the form

$$\mathbf{A}\delta p = \mathbf{b}, \quad (17)$$

which is the linear pressure system and can be solved using any standard linear solver.

After the pressure is updated, the change in porosity is calculated using Eq. 5 and the component accumulation term (denoted $\mathcal{A}_i$) in the mass-balance equation (Eq. 1) is calculated from

$$\mathcal{A}_i^{k+1} = \frac{\phi N_i^k + N_i^k\delta\phi + \phi^k\delta N_i - \phi^n N_i^n}{\Delta t}. \quad (18)$$

In Eq. 18, δN_i has been expressed in terms of δp using the mass-balance equation (Eq. 1). Then, the $(k+1)$th iteration concentrations are obtained using the equation

$$N_i^{k+1} = \frac{\Delta t\mathcal{A}_i^{k+1} + \phi^n N_i^n}{\phi^{k+1}}. \quad (19)$$

Component material-balance errors arise because of the product of N_i^{k+1} and ϕ^{k+1}, and these are avoided by the correction in Eq. 19. The explicit-in-time nature of the concentration in Eq. 19 may cause the IMPEC calculations to become unstable if timesteps become too large. To limit timestep sizes, the simulator currently uses a saturation-type control to limit timestep sizes for the iterative IMPEC implementation. For a given component, saturation change is defined as

$$\left(\Delta S_\Sigma\right)_i = \frac{\partial S_\Sigma}{\partial N_i}\Delta N_i, \quad (20)$$

where ΔN_i is the change in concentration of the ith component. The simulator then requires that $\left|\left(\Delta S_\Sigma\right)_i\right| \leq \Delta S_{\max}$ for all components i during a timestep where $\Delta S_{\max}$ is a user-specified input.

After the $(k+1)$th level iteration solution for p and N_i are available, the simulator returns to check if the volume-balance (convergence) condition given in Eq. 15 is satisfied. If not, it repeats the process described between Eqs. 16 and 19 until Eq. 15 holds up to a tolerance or until a maximum number of iterations is exceeded. At each iteration, the solution from the most recently available iteration (or previous timestep in the case $k = 1$) is used.

Thermal-Energy-Transfer Model

The IPARS model implements a weak or sequential coupling between the flow and thermal steps. For most practical subsurface applications, especially the CO_2-sequestration processes mentioned in the Introduction, this is justifiable because the temperature changes encountered typically are relatively small. In this section, equations governing thermal energy transfer in the time-split solution-scheme steps are presented. Thermal energy balance is described by the partial-differential equation

$$\frac{\partial C_{v,\mathrm{res}}T}{\partial t} + \nabla\cdot\left(\sum_\alpha \rho_\alpha C_{p\alpha}T\mathbf{u}_\alpha - \lambda\nabla T\right) = q_H \quad (21)$$

in the unknown reservoir temperature T, where $C_{v,\mathrm{res}}$ is the effective isochoric specific-heat capacity (in thermodynamics, this is nothing but $\partial U/\partial T$, U being the internal energy). It is given by

$$C_{v,\mathrm{res}} = \left(1-\phi\right)\rho_s C_{vs} + \phi\sum_\alpha \rho_\alpha S_\alpha C_{v\alpha}. \quad (22)$$

In Eqs. 21 and 22, $C_{p\alpha}$ and $C_{v\alpha}$ are the isobaric and isochoric molar specific-heat capacities of Phase α computed from their respective component counterparts using an appropriate mixing rule. The effective reservoir thermal conductivity is denoted by λ, and q_H is the heat source/sink per unit volume, given by

$$q_H = \sum_\alpha C_{p\alpha} q_\alpha T_{src}, \quad (23)$$

where q_α is the injection or production flow rates of Phase α per unit volume, once again calculated from their component counterparts q_i in Eq. 1 and the component mole fractions. It is noted that T_{src} is the temperature of the injected fluid T_{inj} at source points and equals the resident temperature T at the sink points. The subscript s in Eq. 22 represents the rock phase.

Time-Split Scheme. Let $t^{m+1} \in \left[t^n, t^{n+1}\right]$ be the time at which the thermal step is solved. In general, the simulator allows for multiple thermal steps nested within a flow step. The basic idea of the time-split scheme is to account successively (by accumulation) for the advection and diffusion (or thermal conduction, in this case) in time. Hence, it can be regarded as an operator-splitting method. Theoretical details of the method can be found in Dawson and Wheeler (1987) and Peszynska and Sun (2001), where it has been applied to the species-transport problem. Accordingly, Eq. 21 is

split into an advection and a diffusion step. The advection step is given by

$$\frac{\partial\left(C_{v,\mathrm{res}}T\right)}{\partial t}+\nabla\cdot\left(\sum_{\alpha}\rho_{\alpha}C_{p\alpha}T\mathbf{u}_{\alpha}\right)=q_{H}. \quad \ldots\ldots\ldots\ldots\ldots\ldots (24)$$

A higher-order Godunov method has been implemented using element slopes of the scalar variables in the advection term and carefully chosen flux limiters (Eymard et al. 2000; Liu et al. 1994; Dawson 1993). The first-order scheme is presented here. Let E be any element of the finite-element mesh and $H_E^m \equiv \int_E C_{v,\mathrm{res}}^m T^m \mathrm{d}x$ be the local thermal-energy content in E at Timestep m of the thermal algorithm. Integration over E of Eq. 24 against the characteristic function on E gives the weak form of the advection step:

$$\frac{\bar{H}-H_E^m}{\Delta t^m}+\int_E\sum_{\alpha}\bar{\mathbf{u}}_{\alpha}\cdot\mathbf{n}\mathrm{d}s=\int_E q_H^{m+1/2}\mathrm{d}x. \quad \ldots\ldots\ldots\ldots\ldots\ldots (25)$$

In Eq. 25, $\Delta t^m = t^{m+1}-t^m$, $\mathbf{n}$ is the unit outward normal to element E, and $\bar{H}$ denotes the intermediate value of the local thermal-energy content H_E^{m+1} (which is sought to obtain T_E^{m+1}) from the contribution because of advection only and becomes the initial condition for the conduction step. Further, the quantity $\bar{\mathbf{u}}_{\alpha}=\left(C_{p\alpha}T\right)^{m,\mathrm{upw}}\left(\rho_{\alpha}^{\mathrm{upw}}\mathbf{u}_{\alpha}\right)^{m+1/2}$, where $\left(C_{p\alpha}T\right)^{m,\mathrm{upw}}$ represents the upwinded value of $\left(C_{p\alpha}T\right)^m$ on the basis of the sign of $\mathbf{u}_{\alpha}^{m+1/2}\cdot\mathbf{n}$. Similarly, $\rho_{\alpha}^{m+1/2,\mathrm{upw}}$ denotes the upwinded value of $\rho_{\alpha}^{m+1/2}$ on the basis of the sign of $\mathbf{u}_{\alpha}^{m+1/2}\cdot\mathbf{n}$. It is noted that the values of ρ_{α} and $\mathbf{u}_{\alpha}$ are known at flow timesteps t^n and t^{n+1}. Thus, $\left(\rho_{\alpha}\mathbf{u}_{\alpha}\right)^{m+1/2}$ is the linear interpolant computed at $t^{m+1/2}$.

Once $\bar{H}$ is determined, the conduction step is solved, given by

$$\frac{\partial\left(C_{v,\mathrm{res}}T\right)}{\partial t}-\nabla\cdot(\lambda\nabla T)=0. \quad \ldots\ldots\ldots\ldots\ldots\ldots (26)$$

In the weak form, upon integration by the characteristic function on E, this becomes

$$\frac{H_E^{m+1}-\bar{H}}{\Delta t^m}-\int_E\nabla\cdot\left(\lambda\nabla T^{m+1}\right)=0. \quad \ldots\ldots\ldots\ldots\ldots\ldots (27)$$

Eq. 27 is solved using the backward-Euler and mixed-finite-element methods for time and space discretizations, respectively. The lowest order RT_0 approximation space in conjunction with the trapezoidal quadrature rule for the flux term $\lambda\nabla T^{m+1}$ reduces it to a cell-centered finite-difference approximation (Russell and Wheeler 1984). The accumulation term H^{m+1} is linearized about the current temperature. The resulting linear system is solved using the biconjugate gradient method, with the temperature $\bar{T}$ from the advection step as initial guess.

Chemistry Model

After the flow and thermal steps are completed, the chemical reactions are performed. For this purpose, the chemistry component from a separate transport chemistry model (TRCHEM) (Peszynska and Sun 2001) in IPARSv2 was coupled to the thermal/compositional model. At present, the simulator can treat chemical reactions occurring in the aqueous phase that are the most commonly occurring reactions in subsurface-flow applications. First, the ODEs governing chemical reactions are presented. Different types of chemical reactions can be modeled and are briefly described in this section.

Let c_i^{α} represent the concentration of Species i in Phase α, where $c_i^{\alpha}=\xi_i^{\alpha}\rho_{\alpha}S_{\alpha}$. It is noted that c_i^{α} is related to the total concentration N_i by $N_i=\sum_{\alpha}c_i^{\alpha}$. For the chemistry part, α is assumed to be the index corresponding to water phase because only aqueous chemical reactions are considered. Then, let $\mathbf{c}\equiv\{c_i^w\}_{i=1}^{n_c}$ denote the vector of species concentrations in the aqueous phase. Next, suppose that the vector of reaction rates is denoted by $\mathbf{r}(\mathbf{c})$, then the system of nonlinear ODEs governing chemical reaction is given by

$$\frac{\mathrm{d}\mathbf{c}}{\mathrm{d}t}=\mathbf{r}(\mathbf{c}). \quad \ldots\ldots\ldots\ldots\ldots\ldots (28)$$

Multiple chemical-reaction timesteps are allowed in the simulator and are also assumed nested within the flow timestep. The timestep is adjusted when rates of reactions become very large for stability of the solution. Let $\Delta\tau^l \equiv t^{l+1}-t^l$ be the timestep of the chemical reaction where $t^l, t^{l+1}\in\left[t^n, t^{n+1}\right]$. A higher-order explicit RK method of numerical integration is used to solve the system of equations (Eq. 28). The simulator has second- and fourth-order explicit RK methods currently available. For example, using the second-order method (RK2), the formula to update the concentrations of species $i = 1, \ldots, n_c$ from the value $\mathbf{c}$ before the chemistry step to $\hat{\mathbf{c}}$ after the chemistry step is given by

$$\mathbf{k}_{1,i}=\Delta\tau^l\mathbf{r}_i(\mathbf{c}),$$

$$\mathbf{k}_{2,i}=\Delta\tau^l\mathbf{r}_i\left(\mathbf{c}+\frac{1}{2}\mathbf{k}_1\right),$$

and

$$\hat{\mathbf{c}}=\mathbf{c}+\mathbf{k}_2. \quad \ldots\ldots\ldots\ldots\ldots\ldots (29)$$

The coupled flow-thermal-chemistry algorithm is shown in the flow chart of **Fig. 1.**

Reaction Types. The simulator can model kinetic, equilibrium, and Monod-style chemical reactions.

Kinetic Chemical Reactions. Kinetic chemical reactions are modeled using the classical power rate law. Suppose n_{rk} is the number of products formed by kinetic chemical reactions, and let n_{rp} be the total number of products formed by reactions. For each product of the kinetic-reaction type, the kinetic rate is expressed as the difference between the forward and backward reaction rates as

$$r_i=k_{iw}^f\prod_{j=1}^{n_{rc}}\left(c_{jw}\right)^{p_{ji}}-k_{iw}^b c_{n_{rc}+i,w}. \quad \ldots\ldots\ldots\ldots\ldots\ldots (30)$$

In Eq. 30, $i\in I_K$, the index set of the products of kinetic reactions. Next, n_{rc} denotes the number of components entering into chemical reactions (these are numbered first followed by the products $n_{rc}+1, \ldots, n_{rc}+n_{rp}$); k_{iw}^f and k_{iw}^b represent the forward and backward rate constants, respectively, in the aqueous phase; and $p\in\mathbb{R}^{n_{rc}\times n_{rk}}$ denotes the matrix of powers on the components in the rate law.

Monod-Style Chemical Reactions. Monod-style chemical reactions are commonly used to describe biologically mediated reactions such as the reaction between aerobic or anaerobic microbes and nonaqueaous-phase liquid. The growth of the concentration of microbes X on a substrate S is governed by a Monod empirical model of the form

$$\frac{\mathrm{d}[X]}{\mathrm{d}t}=k\frac{[X][S]}{K^h+[S]}, \quad \ldots\ldots\ldots\ldots\ldots\ldots (31)$$

where K^h is the half-saturation constant. Again, letting $i\in I_M$, the index set of the products of Monod reactions, the rate of formation of such products is given by

$$r_i=k_{iw}^f\prod_{j=1}^{n_{rc}}\left(c_{jw}\right)^{p_{ji}}\prod_{j=1}^{n_{rc}}\frac{c_{jw}}{K_{ij}^h+c_{jw}}-k_{iw}^b c_{n_{rc}+i,w}. \quad \ldots\ldots\ldots\ldots\ldots\ldots (32)$$

It is noted that, when $K^h = 0$, the Monod rate (Eq. 31) reduces to a distance-from-equilibrium expression. Typical bio-reactions are irreversible, and the backward-rate constants in Eq. 32 are usually set to zero.

Equilibrium-Style Chemical Reactions. Equilibrium-style chemical reactions are commonly used to model fast chemical

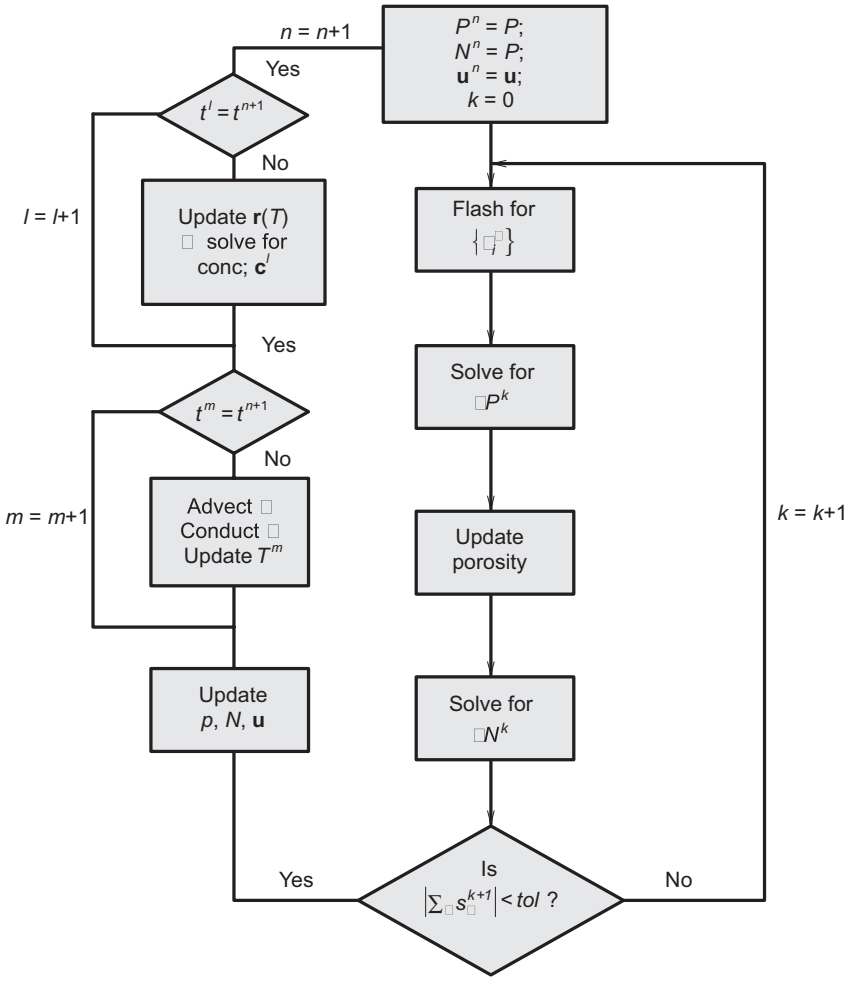

Fig. 1—Coupled flow/thermal/chemistry algorithm.

reactions that proceed in both directions and reach a state of instantaneous chemical equilibrium (i.e., when the forward and backward reactions proceed at the same rate). Let k^f_{iw} and k^b_{iw} denote the forward- and backward-rate constants, respectively; then, equating the two rates in the rate law yields the equilibrium constant $K_{iw} \equiv k^f_{iw} / k^b_{iw}$. The concentration of the products indexed $i \in I_E$, the set of products formed by the equilibrium chemical reactions, are then given by

$$c_{n_{rc}+i,w} = K_{iw} \prod_{j=1}^{n_{rc}} \left(c_{jw}\right)^{a_{ji}} \quad \ldots\ldots\ldots\ldots\ldots\ldots\ldots\ldots\ldots\ldots (33)$$

In Eq. 33, a_{ji} represents stoichiometric coefficients of the reaction. Finally, it is also noted that the rate constants k^f_{iw}, k^b_{iw}, and K_{iw} appearing in Eqs. 30 through 33 are, in general, functions of temperature given by the Arrhenius function $k = A\exp^{-E_a/RT}$, where E_a is the activation energy and R is the universal gas constant. For more theoretical aspects on chemical reactions, see Ostwald (1912).

Computational Results

Model validation tests for isothermal and nonisothermal flow problems were presented in Delshad et al. (2008a, 2008b). In this section, the numerical model presented in the preceding sections is tested on some challenging problems. The first problem is designed to illustrate the parallel performance of the flow model on extremely fine grids and heterogeneous permeability fields. It also motivates the use of an iteratively coupled flow model for multiphase, multicomponent EOR applications, as opposed to a fully implicit method. The second problem demonstrates the application of the coupled flow and thermal model to solve the problem of CO_2 flow and leakage when injected close to an abandoned leaky well. The final example presents the coupling of flow, thermal, and chemistry applied to CO_2 injection in a deep heterogeneous aquifer.

Large-Scale Parallel Computations. This example simulates a multiphase-flow scenario in which a five-spot water-alternating-gas (WAG) injection cycle with the injection well located at the center of the domain and the production wells at the four corners is employed for oil production. Primary production is carried out during the first year, followed by water injection at 12,000 STB/D alternated with gas injection at 12,000 Mscf/D thereafter with a period of 1 year each. The nonaqueous phases are assumed to consist of six components, the *n*-alkanes, C_1, C_3, C_6, C_{15}, and C_{20}. Gas injection is proportioned among the first three components as 77% methane, 20% propane, and 3% hexane. An extremely heterogeneous reservoir with permeabilities varying by six orders of magnitude and derived from the Tenth SPE Comparative Solution Project is assumed (Christie and Blunt 2001) after projecting onto a very fine grid of 100×100×40. The global dimensions of the reservoir are 3500×3500×100 m. Isothermal-flow conditions are assumed at a reservoir temperature T = 160°F. The simulation time is 3 years. The rock properties, initial composition of the reservoir, and phase behavior have been derived from the Fifth SPE Comparative Solution Project (Killough and Kossack 1987), which was described on a very coarse grid (3×7×7). The original coarse-grid problem was prescribed as a uniform permeability field. The results of the coarse-grid problem were first successfully matched against a commercial simulator before attempting to solve the modified fine-grid problem described here.

For a fully implicit implementation, the number of unknowns for this problem per element is 7 after elimination of secondary

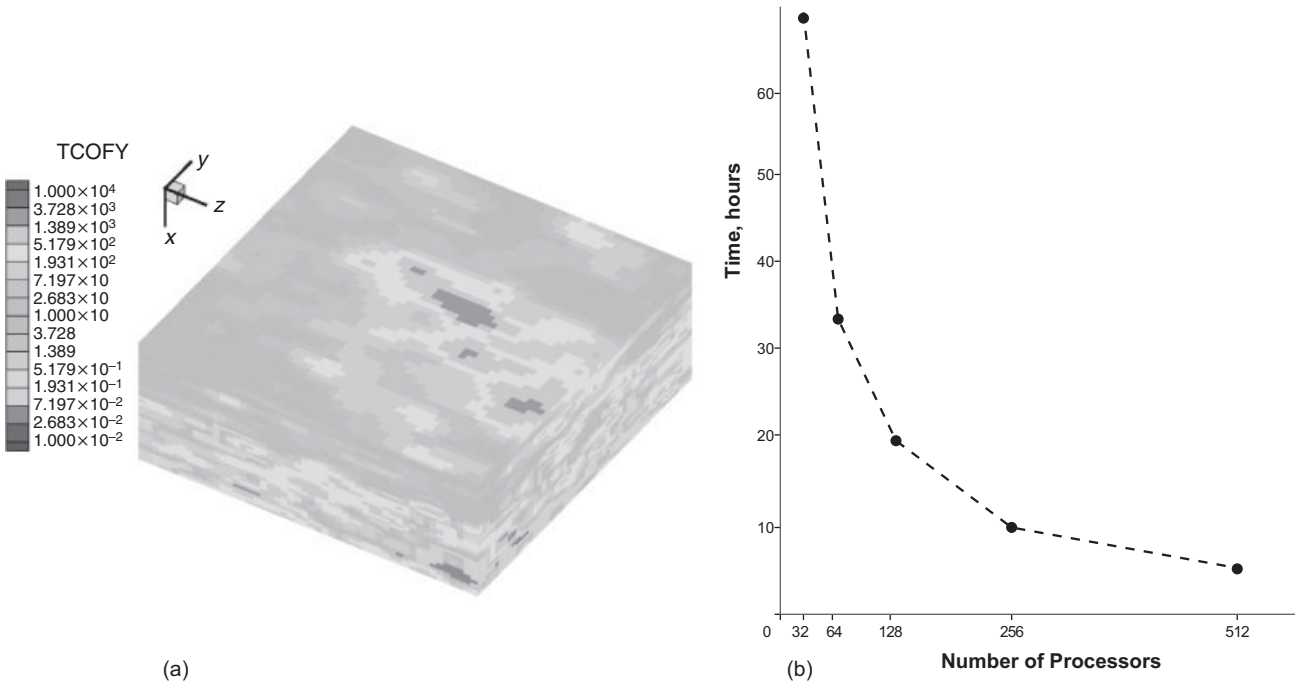

Fig. 2—Permeability field and parallel performance.

unknowns such as fugacities [(Coats 1980), see, for example, Eq. 26 and the discussion preceding it, therein]—i.e., one for the reference-phase pressure and one for each of the six hydrocarbon-component molar concentrations. Hence, the Jacobian computations are excessively expensive (Chen et al. 2000). On extremely fine grids, such as those used in this simulation, this could potentially become extremely difficult to solve using codes that implement fully implicit compositional models. This problem was tested on 32, 64, 128, 256, and 512 processors on the parallel distributed memory architecture of the Lonestar cluster at the Texas Advanced Computing Center (TACC) facility at The University of Texas at Austin. A parallel efficiency of approximately 80% (at 512 processors) is observed. **Figs. 2a and 2b** show the K_{yy} permeability field in millidarcies and the parallel performance (plot of actual computational time vs. number of cores), respectively. The gas saturation and molar concentration of a component (propane) at the end of one complete WAG cycle (i.e., 3 years) are shown in **Figs. 3a and 3b,** respectively.

Parallel Simulations of CO_2 Sequestration. This example simulates the leakage of CO_2 when injected near an abandoned leaky well. The physical reservoir is a domain of dimensions 1000×1000×160 m. There are two aquifers of permeability of approximately 20 md each, separated by an impermeable aquitard. A leaky well modeled as a porous medium with a permeability of approximately 1000 md is located at the center of the domain, and an injection well is 100 m away. CO_2 is injected at a rate of 8.8 kg/s at 92.48°F. The reservoir is initially saturated with brine and is at a depth of 640 m. An initial geothermal gradient of 0.054 °F/m is specified with a bottom temperature of 93.2°F. The outputs of interest were the CO_2-leakage rate at the midsection of the leaky well (as a percent of the injection rate), the CO_2-plume shape as it approached the leaky well, the arrival time, and the peak leakage value. The boundary conditions were no-flow on the vertical surfaces and equal to the initial conditions on the lateral surfaces. A schematic of the problem is shown in **Fig. 4.**

Because of the shallow depth of the reservoir, the critical pressure and temperature of CO_2 happen to lie along the midplane passing through the aquitard. As a result of this, when CO_2 rises, it experiences large changes in properties, which combined with the varying spatial and temporal reservoir temperature, in turn, have a strong influence on the leakage rate. Brooks-Corey (1964)

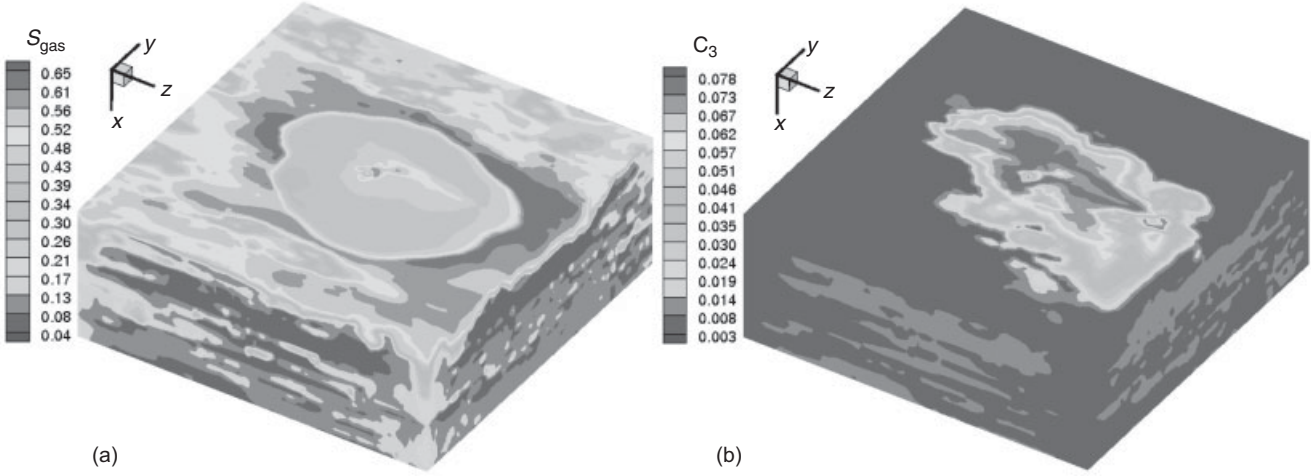

Fig. 3—Gas saturation and C_3 molar concentration.

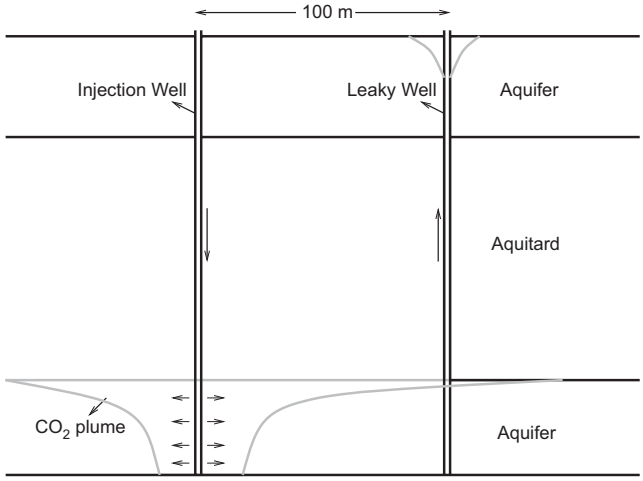

Fig. 4—CO_2 injected near an abandoned leaky well.

relative permeability and capillary pressure curves are assumed. **Figs. 5a and 5b** show the CO_2-leakage rate and temperature in the leaky well, respectively. The sudden drop in temperature when CO_2 initially reaches the leaky well is because of the displacement of warmer brine and abrupt change in properties upon crossing the critical point.

An arrival time of close to 50 days is observed, which agreed reasonably well with other comparable commercial and academic research codes (Class et al. 2009). A simulation on a similar problem with a greater reservoir depth of 2840 m, isothermal conditions, and a linear relative permeability and capillary pressure produced earlier arrival time and higher leakage rates. **Figs. 6a and 6b** show the CO_2 gas saturation and reservoir-temperature profile, respectively, across a section passing through the wells at t = 705 days. This problem was solved using a computational grid of 66×45×64 on up to 96 processors on the Ranger cluster at TACC and the Bevo2 cluster at the Institute for Computational Engineering and Sciences at The University of Texas at Austin.

Coupled Flow/Thermal/Chemistry Example. The last example presents a serial simulation of the coupling of nonisothermal flow and chemistry as applied to problems in CO_2 sequestration. In this

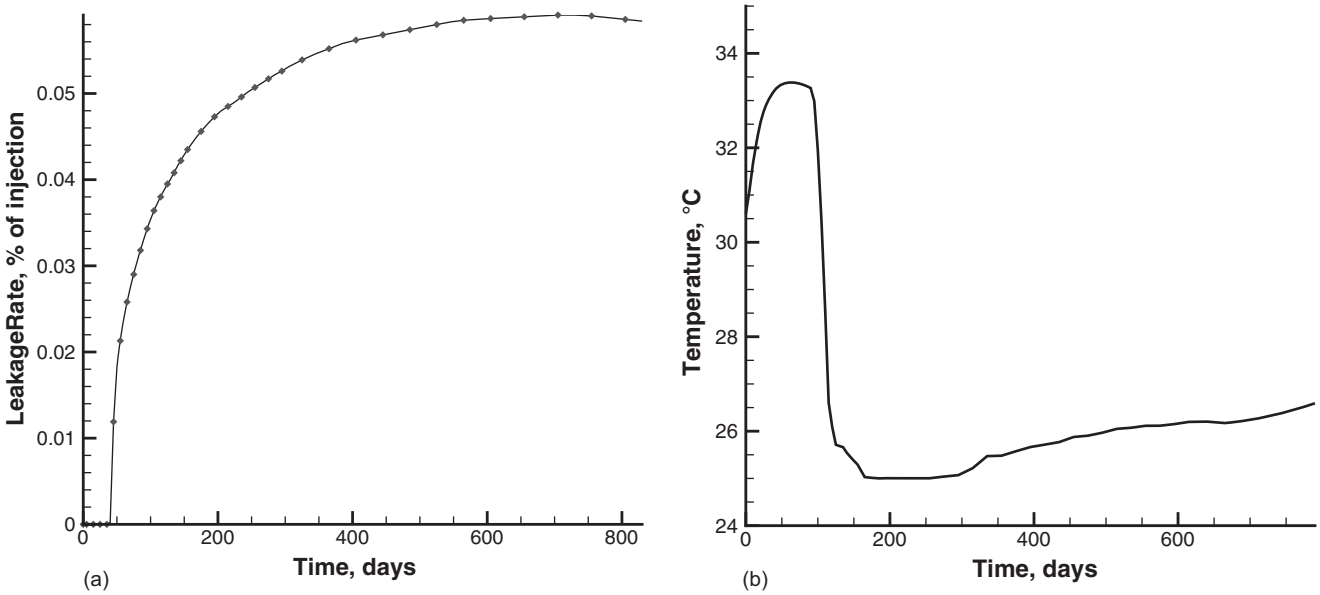

Fig. 5—CO_2 leakage rate and temperature profile in leaky well.

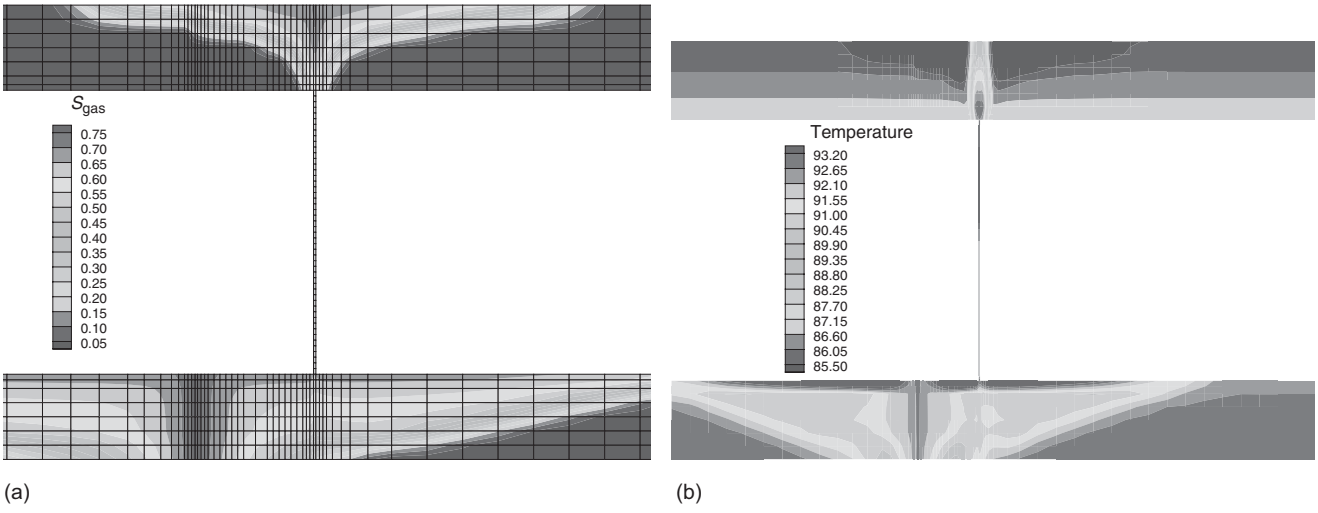

Fig. 6—CO_2 saturation and reservoir temperature across a section through wells.

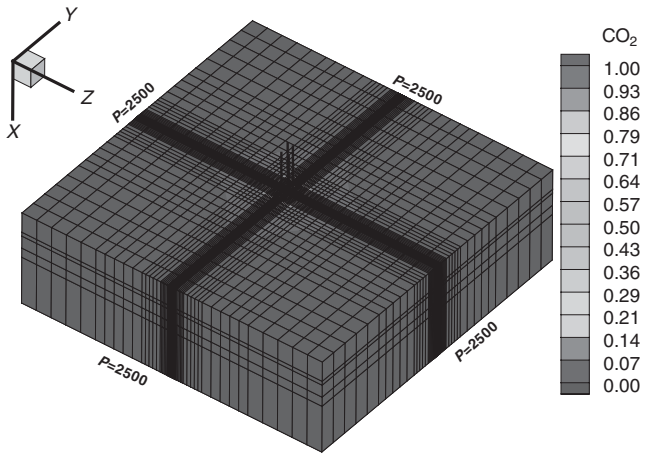

(a)

(b)

Fig. 7—CO_2 injection in a deep aquifer and temperature across section through two wells.

problem, CO_2 is injected to a deep aquifer at 5000-m depth by four wells located in a square located at the center of a domain with physical dimensions of 325,000×325,000×256 ft. The problem models flow of two phases (CO_2 and H_2O) and three components (H_2O, CO_2, and H_2CO_3). The CO_2 is injected for 10 years at 75,000 Mscf/D at a temperature of 176°F. The initial reservoir temperature is 200°F. The reservoir is assumed to have a layered permeability field. A fine grid of 50×50×5 is used in the computation. An equilibrium chemical reaction of the form $H_2O+CO_2 \rightleftharpoons H_2CO_3$ governs the formation of H_2CO_3. The goal was to study the distribution of CO_2 and H_2CO_3 and the reservoir-temperature profile at the end of 10 years' simulation time.

Fig. 7a shows the computational domain with grid and well locations superimposed. A fine grid is used around the wells. Fig. 7b shows the reservoir temperature in a section passing through two of the wells. Because of the aereal symmetry of the reservoir, as well as the symmetry of the well location, the solution is similar in all cross sections passing through any two adjacent wells. It is observed that the temperature is reduced from 200 to 176°F around the injection wells. Finally, **Figs. 8a and 8b** show the CO_2 and H_2CO_3 molar concentrations, respectively, after the 10-year simulation period in a close-up across a section passing through two of the wells. Because of the layered permeability field, the transport and reaction plumes form fingers spreading in a nonuniform manner with depth.

Nomenclature

A_α = parameter in Peng-Robinson EOS of Phase α
B_α = parameter in Peng-Robinson EOS of Phase α
$\mathbf{c}$ = vector of aqueous-phase species concentrations
c_r = rock compressibility
$C_{p\alpha}$ = isobaric specific heat of Phase α
$C_{v,\,\mathrm{res}}$ = effective reservoir isochoric specific heat
$C_{v\alpha}$ = effective isochoric specific heat of Phase α
C_α = volumetric shift in Peng-Robinson EOS of Phase α
$\mathbf{D}_i^\alpha$ = diffusion/dispersion tensor of Species i in Phase α
f_i^α = fugacity of Species i in Phase α
$h_{1(2,\,3)}$ = coefficients in cubic Peng-Robinson EOS of Phase α
H^k = thermal content in Cell E at Timestep k
$\mathbf{J}_i^\alpha$ = net velocity of Species i in Phase α
$\mathbf{K}$ = medium absolute permeability
K_i = ratio of ξ_i^g to ξ_i^l
$n_c(n_p)$ = number of components/species (phases)
N_i = molar concentration of Component i
$p_{c\alpha}$ = capillary pressure of Phase α
p_α = pressure of Phase α
q_H = external source/sink of heat
q_i = sources/sinks of Component i in flow
R = universal gas constant
R_i = residual of flash equilibrium for Species i
$\mathbf{r}$ = vector of reaction rates
S_α = saturation of Phase α
$\{S_\alpha\}$ = set of all phase saturations, $\alpha = 1, \ldots, n_p$
S_Σ = sum of phase saturations
T = reservoir temperature
$\mathbf{u}_\alpha$ = Darcy velocity of Phase α
v = vapor fraction of fluid composition
v_α = molar specific volume of Phase α
z_i = overall nonaqueous mole fraction of Species i
Z_α = compressibility (or Z factor) of Phase α
γ_α = specific gravity of Phase α; i.e., $\equiv \rho_{\alpha g}$
$\kappa_{r\alpha}$ = relative permeability of Phase α

(a)

(b)

Fig. 8—CO_2 and H_2CO_3 concentrations across section passing through two wells.

λ = effective reservoir thermal conductivity
μ_α = viscosity of Phase α
ξ_i^α = mole fraction of Species i in Phase α
$\{\xi_i\}^\alpha$ = set of all ξ_i^α for fixed Phase α
ρ_α = density of Phase α
ϕ = medium porosity
Φ_i^α = fugacity coefficient of Species i in Phase α

Acknowledgments

The authors were partially supported by the National Science Foundation grant DMS 0618679 and by the US Department of Energy grant DE-FG02-04ER25617. The authors also acknowledge the contribution of R.H. Dean to the development of the legacy flow model source code as well as the contribution of J.A. Wheeler to the development of the IPARSv3 reservoir-simulator framework.

References

Acs, G., Deleschall, S., and Farkas, E. 1985. General Purpose Composition Model. *SPE J.* **25** (4): 543–553. SPE-10515-PA. doi: 10.2118/10515-PA.

Bachu, S. 2000. Sequestration of CO_2 in Geological Media: Criteria and Approach for Site Selection in Response to Climate Change. *Energy and Conversion Management* **41** (9): 953–970. doi: 10.1016/S0196-8904(99)00149-1.

Brantferger, K.M., Pope, G.A., and Sepehrnoori, K. 1991. Development of a Thermodynamically Consistent, Fully Implicit, Equation-of-State, Compositional Steamood Simulator. Paper SPE 21253 presented at the SPE Symposium on Reservoir Simulation, Anaheim, California, USA, 17–20 February. doi: 10.2118/21253-MS.

Brooks, A.N. and Corey, A.T. 1964. Hydraulic Properties of Porous Media. Hydrology Paper 3, Colorado State University, Fort Collins, Colorado.

Chang, Y.-B. 1990. Development and Application of an Equation of State Compositional Simulator. PhD dissertation, University of Texas at Austin, Austin, Texas (August 1990).

Chen, Z., Ewing, R.E., and Qin, G. 2000. Analysis of a Compositional Model for Fluid Flow in Porous Media. *SIAM J. Appl. Math* **60** (3): 747–777. doi: 10.1137/S0036139998333427.

Chen, Z., Huan, G., and Ma, Y. 2006. *Computational Methods for Multiphase Flows in Porous Media*. Philadelphia, Pennsylvania: Society for Industrial and Applied Mathematics (SIAM).

Chen, Z., Huan, G., and Wang, H. 2005. Simulation of a Compositional Model for Multiphase Flow in Porous Media. *Numerical Methods for Partial Differential Equations* **21** (4): 726–741. doi: 10.1002/num.20059.

Chen, Z., Ma, Y., and Chen, G. 2007. A Sequential Numerical Chemical Compositional Simulator. *Transport in Porous Media* **68** (3): 389–411. doi: 10.1007/s11242-006-9050-y.

Christie, M.A. and Blunt, M.J. 2001. Tenth SPE Comparative Solution Project: A Comparison of Upscaling Techniques. *SPE Res Eval & Eng* **4** (4): 308–317. SPE-72469-PA. doi: 10.2118/72469-PA.

Class, H., Ebigbo, A., Helmig, R., Dahle, H.K., Nordbotten, J.M., Celia, M.A., Audigane, P. et al. 2009. A Benchmark Study on Problems Related to CO_2 Storage in Geologic Formations. *Computational Geosciences* **13** (4): 409–434. doi: 10.1007/s10596-009-9146-x.

Coats, K.H. 1980. An Equation of State Compositional Model. *J Pet Technol* **20** (5): 363–376. SPE-8284-PA. doi: 10.2118/8284-PA.

Dawson, C. 1993. Godunov-Mixed Methods for Advection-Diffusion Equations in Multidimensions. *SIAM J. Numer. Anal.* **30** (5): 1315–1332. doi: 10.1137/0730068.

Dawson, C.N. and Wheeler, M.F. 1987. An Operator-Splitting Method for Advection-Diffusion-Reaction Problems. In *The Mathematics of Finite Elements and Applications VI*, ed. J.R. Whiteman, 463–482. London, UK: Academic Press.

Delshad, M., Pope, G.A., and Sepehrnoori, K. 2000. UTCHEM version 9.0 technical documentation. CPGE, The University of Texas at Austin, Austin, Texas (July 2000).

Delshad, M., Thomas, S.G., and Wheeler, M.F. 2008. Modeling CO_2 Sequestration Using a Sequentially Coupled "Iterative-IMPEC-Time-Split-Thermal" Compositional Simulator. Presented at the 11th European Conference on the Mathematics of Oil Recovery (ECMOR XI), Bergen, Norway, 8–11 September.

Delshad, M., Thomas, S.G., and Wheeler, M.F. 2008. Parallel Simulations of CO_2 Sequestration Using a Non-Isothermal Compositional Model. Accepted for presentation at the 2008 ASME International Mechanical Engineering Congress and Exposition (IMECE), Boston, Massachusetts, USA, 2–6 November.

Eymard, R., Gallouët, T., and Herbin, R. 2000. Finite Volume Methods. In *Handbook of Numerical Analysis VII*, ed. P.G. Ciarlet and J.L. Lions, 713–1020. Amsterdam, The Netherlands: Elsevier B.V.

Firoozabadi, A. 1999. *Thermodynamics of Hydrocarbon Reservoirs*. New York: McGraw-Hill.

Killough, J.E. and Kossack, C.A. 1987. Fifth Comparative Solution Project: Evaluation of Miscible Flood Simulators. Paper SPE 16000 presented at the SPE Symposium on Reservoir Simulation, San Antonio, Texas, USA, 1–4 February. doi: 10.2118/16000-MS.

Liu, J., Delshad, M., Pope, G.A., and Sepehrnoori, K. 1994. Application of Higher-Order Flux-Limited Methods in Compositional Simulation. *Transport in Porous Media* **16** (1): 1–29. doi: 10.1007/BF01059774.

Model Testing With Benchmark Examples Developed in the Project "Numerical Investigation of CO_2 Sequestration in Geological Formations—Problem-Oriented Benchmarks." 2008. Workshop on Numerical Models for Carbon Dioxide Storage in Geological Formations, Stuttgart, Germany, 2–4 April, http://www.iws.uni-stuttgart.de/co2-workshop.

Ostwald, W. 1912. *Outlines of General Chemistry*, third edition, trans. W.W. Taylor. London, UK: MacMillan & Co.

Peng, D.-Y. and Robinson, D.B. 1976. A New Two-Constant Equation of State. *Ind. Eng. Chem. Fundamentals* **15** (1): 59–64. doi: 10.1021/i160057a011.

Peszynska, M. and Sun, S. 2001. Multiphase Reactive Transport Module (TRCHEM) in IPARS. Technical Report ICES 01-32, Texas Institute for Computational and Applied Mathematics, The University of Texas at Austin, Austin, Texas (October 2001).

Russell, T.F. and Wheeler, M.F. 1984. Finite Element and Finite Difference Methods for Continuous Flows in Porous Media. In *The Mathematics of Reservoir Simulation*, ed. R.E. Ewing, Vol. 1, 35–106. Philadelphia, Pennsylvania: Frontiers in Applied Mathematics, SIAM.

Watts, J.W. 1986. A Compositional Formulation of the Pressure and Saturation Equations. *SPE Res Eng* **1** (3): 243–252; *Trans.,* AIME, **281.** SPE-12244-PA. doi: 10.2118/12244-PA.

Wheeler, M.F. 2001. Advanced Techniques and Algorithms for Reservoir Simulation, II: The Multiblock Approach in the Integrated Parallel and Accurate Reservoir Simulator (IPARS). Technical Report ICES 01-25, Texas Institute for Computational and Applied Mathematics, University of Texas at Austin, Austin, TX (01 September 2001).

Mojdeh Delshad is a research associate professor in the Department of Petroleum and Geosystems Engineering and a visiting research associate professor and assistant director of the Center for Subsurface Modeling at The Institute for Computational Engineering and Sciences at The University of Texas at Austin. She holds a PhD degree in petroleum engineering from The University of Texas at Austin. Delshad's research interests and areas of expertise include reservoir engineering, modeling petrophysical properties, simulation of chemical and CO_2EOR processes, modeling of wettability alteration by use of chemicals to improve oil production from fractured carbonate formations, and numerical simulations of CO_2 storage in deep saline aquifers. She is in charge of the development and user support of UTCHEM, The University of Texas chemical flooding simulator, for modeling chemical and transport phenomena in the subsurface, in which she has more than 15 years of experience. **Sunil G. Thomas** works in the Reservoir Simulation Development division at Chevron ETC in San Ramon, Clifornia. He holds a PhD degree in computational mathematics from The University of Texas at Austin. Thomas' research interests and areas of expertise lie in parallel domain decomposition methods for multiphase flow and iterative coupled systems for flow and transport through subsurface porous media. In addition, he has expertise in the implementation and application of parallel stochastic inverse modeling algorithms for reservoir characterization and history matching as well as in multiphysics coupling of different numerical discretization methods on nonmatching multiblock grids. Thomas' more recent work includes extension of the analysis and implementation of multiblock techniques, such as enhanced velocity mixed finite element

methods to coupled flow transport systems in porous media applications. **Mary F. Wheeler** holds the Ernst Virginia Cockrell Chair of Engineering at The University of Texas at Austin and is a professor in the Departments of Mathematics, Petroleum and Geosystems Engineering, and Aerospace Engineering and Engineering Mechanics. She holds a PhD degree in mathematics from Rice University. Wheeler is the director of the Center for Subsurface Modeling at the Institute for Computational Engineering and Sciences at The University of Texas at Austin. She is a member of the National Academy of Engineering. Wheeler pioneered the analysis, understanding, and application of the theory of finite elements in subsurface applications during the last 4 decades. She is a leading expert in the theory of numerical methods for reservoir simulation, such as mixed finite elements, its analogies to different cell-centered finite difference and finite volume approximations in reservoir simulation, discontinuous Galerkin methods, domain decomposition methods, iterative coupling timestepping methods for multiphase and compositional flow, multinumerics and multiscale couplings of multiphysics applications, autonomic reservoir management and history matching, and several other areas of applications. Wheeler has published hundreds of articles in leading journals and remains an active influence in these areas of research.